Journal of Materials Chemistry C

PAPER

View Article Online
View Journal | View Issue

Cite this: J. Mater. Chem. C, 2016, 4, 1336

Structure and luminescence properties of Eu^{2+} doped $Lu_xSr_{2-x}SiN_xO_{4-x}$ phosphors evolved from chemical unit cosubstitution

Zhiguo Xia,*[a] Shihai Miao,[b] Maxim S. Molokeev,[cd] Mingyue Chen[a] and Quanlin Liu[a]

Received 12th December 2015,
Accepted 12th January 2016

DOI: 10.1039/c5tc04222d

www.rsc.org/MaterialsC

The design scheme of the chemical unit cosubstitution of $[Lu^{3+}–N^{3-}]$ for $[Sr^{2+}–O^{2-}]$ in $Sr_2SiO_4:Eu^{2+}$ has been put into practice to discover the new phosphor systems with tunable luminescence properties, and the structures and photoluminescence tuning of yellow-emitting $Lu_xSr_{2-x}SiN_xO_{4-x}:Eu^{2+}$ phosphors have been investigated. Crystal structures of $Lu_xSr_{2-x-y}SiN_xO_{4-x}:yEu^{2+}$ samples were resolved using the Rietveld method, suggesting that the as-prepared Sr_2SiO_4 belonged to monoclinic symmetry ($P2_1/n$) of β-phase Sr_2SiO_4, while $Sr_{1.97}Eu_{0.03}SiO_4$ and $Sr_{1.965}Eu_{0.03}Lu_{0.005}SiO_{3.995}N_{0.005}$ belonged to orthorhombic symmetry (*Pnma*) of α-Sr_2SiO_4. The emission peaks of $Lu_xSr_{1.97-x}SiN_xO_{4-x}:0.03Eu^{2+}$ phosphors were red-shifted from 563 to 583 nm upon increasing the $[Lu^{3+}–N^{3-}]$ substitution content from $x = 0$ to $x = 0.005$, furthermore, the PL emission peaks of $Lu_{0.005}Sr_{1.965-y}SiN_{0.005}O_{3.995}:yEu^{2+}$ also showed a red-shift from 583 nm to 595 nm with increasing Eu^{2+} concentration ($y = 0.03$, 0.07, 0.10 and 0.15), and their corresponding red-shift mechanism has been discussed. The temperature dependent luminescence results further verified that the introduction of $[Lu^{3+}–N^{3-}]$ for $[Sr^{2+}–O^{2-}]$ in $Sr_2SiO_4:Eu^{2+}$ can improve the thermal stability of the photoluminescence, which indicated that the $Lu_xSr_{2-x-y}SiN_xO_{4-x}:yEu^{2+}$ phosphors have potential applications in white light-emitting diodes (wLEDs).

1. Introduction

The discovery of new inorganic materials is always a hot issue in solid-state materials chemistry and is an important objective highlighted by the "Materials Genome Initiative".[1,2] To establish suitable strategies discovering new host materials for advanced optical materials, many conventional or modified approaches have been developed, such as cation/anion replacement in the single site of the inorganic phases,[3,4] prototype substitution from an original "old" phase to find out a "new" one,[5,6] combinatorial chemistry screening *via* the phase diagram,[7,8] the single-particle-diagnosis approach along with the advanced measurement devices,[9] and our recently reported chemical unit cosubstitution strategy for photoluminescence tuning,[10] and so on. These strategies used for the discovery of the new phosphors demonstrated great success, and many important phosphors have been reported and used finally. Nevertheless, increasingly demanded by newly developed optical materials and devices, phosphors with tunable optical properties are continuously pursued by chemists or material scientists.

Recently, the exploration of new materials for white light-emitting diodes (wLEDs) has become a hot issue.[11,12] Among them, silicate phosphors represented by Eu^{2+} or Ce^{3+} doped orthosilicates A_2SiO_4 (A = Ca, Sr, Ba) have drawn much attention owing to their versatile polymorphs and chemical compositions, broad excitation/emission bands and tunable optical properties.[13,14] As we know, crystal site engineering can be used to tune the luminescence properties by changing the coordination environment for phosphors employing Ce^{3+} or Eu^{2+} ions characterized by d–f transitions. Therefore, the nitridation of the orthosilicate phosphors has demonstrated great potential.[15–23] For example, Sohn reported the $Sr_2SiO_{4-x}N_{2x/3}:Eu^{2+}$ phosphors.[15] Gu reported the N doped $Sr_2SiO_4:Eu^{2+}$ phosphors.[16] Lee reported the $(Sr,M)_2Si(O_{1-x}N_x)_4:Eu^{2+}$ (M: Mg^{2+}, Ca^{2+}, Ba^{2+}) phosphors.[17] Zhao found the red-emitting oxonitridosilicate phosphors $Sr_2SiN_2O_{4-1.5z}:Eu^{2+}$.[18] Park reported the effects of N^{3-}, Eu^{2+}, and Ca^{2+} substitutions on the structural and luminescence properties of $Sr_2SiO_4:Eu^{2+}$.[19] Ju reported the modification of the coordination environment of Eu^{2+} in $Sr_2SiO_4:Eu^{2+}$ phosphors to achieve full color emission.[20] Li reported the luminescence properties and the crystal structure of

[a] The Beijing Municipal Key Laboratory of New Energy Materials and Technologies, School of Materials Sciences and Engineering, University of Science and Technology Beijing, Beijing 100083, China. E-mail: xiazg@ustb.edu.cn; Fax: +86-10-8237-7955; Tel: +86-10-8237-7955
[b] School of Materials Sciences and Technology, China University of Geosciences, Beijing 100083, China
[c] Laboratory of Crystal Physics, Kirensky Institute of Physics, SB RAS, Krasnoyarsk 660036, Russia
[d] Department of Physics, Far Eastern State Transport University, Khabarovsk, 680021, Russia

α-$Sr_2Si_{3x/4}O_2N_x$:Eu^{2+} phosphors with different concentrations of N^{3-} ions.[21] Tian reported the optical spectrum adjustment of yellow-green $Sr_{1.99}SiO_{4-3x/2}N_x$:$0.01Eu^{2+}$ phosphor.[22]

Recently, Black found the new $LaSrSiO_3N$ and $LaBaSiO_3N$ phases, and these compounds activated with Eu^{2+} showed orange-red emission.[23] Such an example is in accord with our previously reported chemical unit cosubstitution strategy,[10] so that the [La^{3+}–N^{3-}] chemical unit can be used to cosubstitute for the [Sr^{2+}/Ba^{2+}–O^{2-}] couple in the $(Sr,Ba)_2SiO_4$:Eu^{2+} phosphors. This is also the main topic highlighted in the present paper, and it is believed that such a strategy can be successfully used to discover the new phosphor materials and tune the luminescence properties. Therefore, the usage and verification of the design scheme of chemical unit cosubstitution will be significant in discovering other new solid state materials. Herein, the chemical unit cosubstitution of [Lu^{3+}–N^{3-}] for [Sr^{2+}–O^{2-}] in Sr_2SiO_4:Eu^{2+} has been proposed in this paper, and the yellow-emitting $Lu_xSr_{2-x}SiN_xO_{4-x}$:Eu^{2+} phosphors with tunable photoluminescence have been studied. As also mentioned above, the nitridation of the orthosilicate phosphors brings us some opportunities to search for new phosphors. In this work, we studied the phase structure evolution and luminescence properties of yellow-emitting $Lu_xSr_{2-x-y}SiN_xO_{4-x}$:$yEu^{2+}$ phosphors, and the observed spectral red-shift with increasing [Lu^{3+}–N^{3-}] and Eu^{2+} content has been discussed in detail.

2. Experimental

The designed $Lu_xSr_{1.97-x-y}SiN_xO_{4-x}$:$yEu^{2+}$ phosphors were synthesized by a conventional high temperature solid-state reaction. The starting materials were as follows: $SrCO_3$ (A.R.), SiO_2 (A.R.), Lu_2O_3 (A.R.), Si_3N_4 (99.99%), and Eu_2O_3 (99.99%). After mixing and grinding in an agate mortar for 20 min, the mixture was placed in a crucible and then sintered at 1500 °C for 4 h in a H_2(10%)/N_2(90%) reducing atmosphere to produce the final samples. Finally, the prepared phosphors were cooled to room temperature and reground for further measurements.

The powder X-ray diffraction (XRD) measurements were performed on a D8 Advance diffractometer (Bruker Corporation, Germany) operating at 40 kV and 40 mA with Cu Kα radiation (λ = 1.5406 Å). The scanning rate for phase identification was fixed at 4° min^{-1} with 2θ ranges from 10° to 70° and the data for Rietveld analysis were collected in a step-scanning mode with

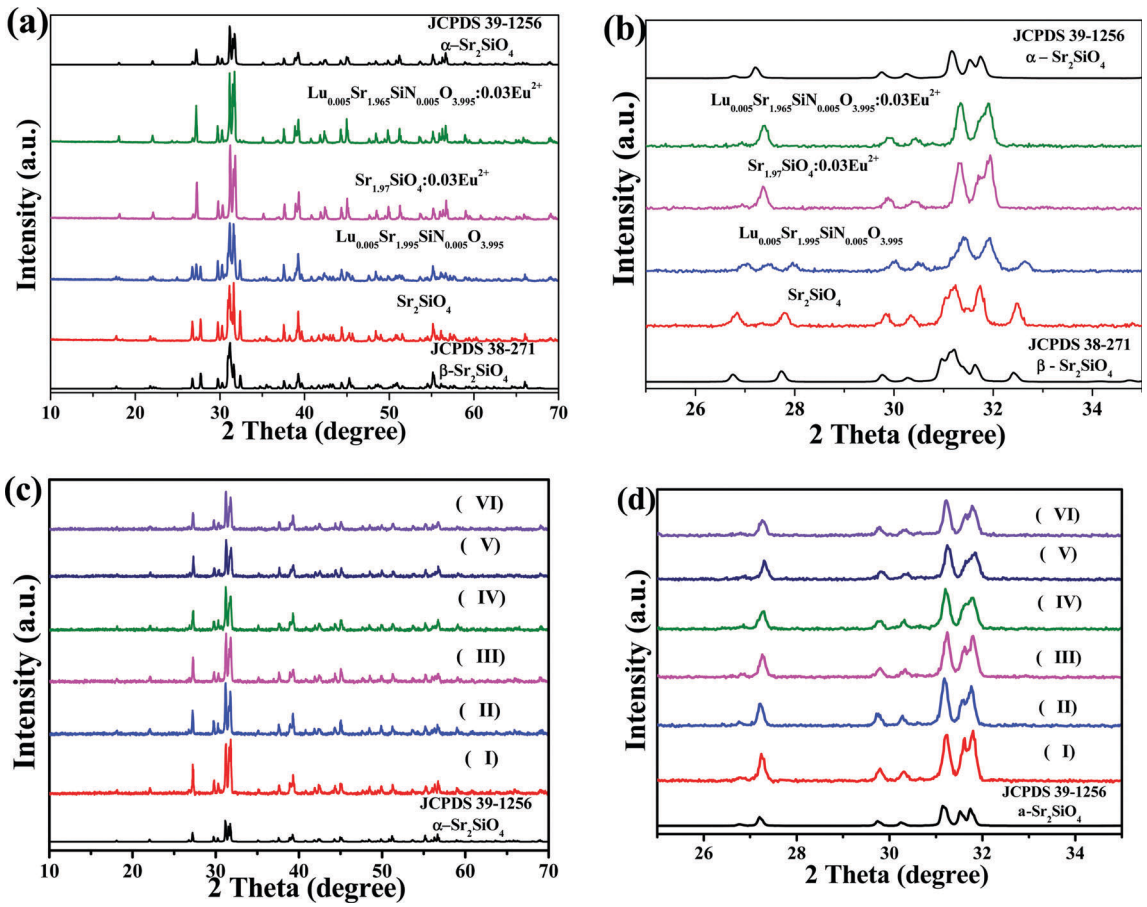

Fig. 1 Full range XRD patterns (a) and the magnified range between 25° and 35° (b) of as-prepared Sr_2SiO_4, $Lu_{0.005}Sr_{1.995}SiN_{0.005}O_{3.995}$, $Sr_{1.97}SiO_4$:$0.03Eu^{2+}$ and $Lu_{0.005}Sr_{1.965}SiN_{0.005}O_{3.995}$:$0.03Eu^{2+}$ samples, and full range XRD patterns (c) and the magnified range between 25° and 35° (d) of $Lu_{0.005}Sr_{1.995-y}SiN_{0.005}O_{3.995}$:$yEu^{2+}$ (y = 0.03 (I), 0.05 (II), 0.07 (III), 0.10 (IV), 0.15 (V) and 0.20 (VI)) phosphors. The standard data for α-Sr_2SiO_4 (JCPDS 39-1256) and β-Sr_2SiO_4 (JCPDS 38-271) are shown as a reference.

the step size of 0.02° and 10 s counting time per step over the 2θ range from 10° to 120°. The morphology and chemical compositions have been detected by using the scanning electron microscopy (SEM, JEOL JSM-6510A) and the attached energy disperse spectroscopy (EDS) techniques. The PL and photoluminescence excitation (PLE) spectra were recorded using a Hitachi F-4600 spectrophotometer (HITACHI, Tokyo, Japan) equipped with a 150 W xenon lamp as the excitation source. The temperature-dependent luminescence properties were also measured on the same spectrophotometer, and it was combined with a self-made heating attachment and a computer-controlled electric furnace (Tianjin Orient KOJI Co., Ltd, TAP-02). The decay curves were recorded on an instrument (Edinburgh Instruments Ltd, UK) (FLSP920) with an F900 flash lamp as the excitation source.

3. Results and discussion

The full range XRD patterns and the magnified range between 25° and 35° of as-prepared Sr_2SiO_4, $Lu_{0.005}Sr_{1.995}SiN_{0.005}O_{3.995}$, $Sr_{1.97}SiO_4$:0.03Eu^{2+} and $Lu_{0.005}Sr_{1.965}Si\ N_{0.005}O_{3.995}$:0.03$Eu^{2+}$ samples are given in Fig. 1a and b, respectively. The standard data for α-Sr_2SiO_4 (JCPDS 39-1256) and β-Sr_2SiO_4 (JCPDS 38-271) are also shown as a reference. From Fig. 1a and b, we can see that the as-obtained Sr_2SiO_4 and $Lu_{0.005}Sr_{1.995}SiN_{0.005}O_{3.995}$ samples can be indexed to the β-Sr_2SiO_4 phase (JCPDS 38-271) suggesting that the introduction of the [Lu^{3+}–N^{3-}] chemical unit in a small amount (x = 0.005) will not affect the phase transition. Moreover, we can find that diffraction peaks of the as-prepared $Lu_{0.005}Sr_{1.995}SiN_{0.005}O_{3.995}$ sample shift to the high-angle direction compared to that of the as-obtained Sr_2SiO_4 phase, which verified that the Lu–N dopant can enter the structural framework of the β-Sr_2SiO_4 phase leading to the shrinkage of the unit cell. However, the impurities appear when the contents of the [Lu^{3+}–N^{3-}] chemical unit exceed x = 0.005 from our experimental results. So that we select the content of x = 0.005 for the following discussion. Furthermore, Fig. 1c and d displays the full range XRD patterns and the magnified range between 25° and 35° for the as-prepared $Lu_{0.005}Sr_{1.995-y}SiN_{0.005}O_{3.995}$:$yEu^{2+}$ (y = 0.03, 0.05, 0.07, 0.10, 0.15 and 0.20) phosphors. The standard data for α-Sr_2SiO_4 (JCPDS 39-1256) are shown as a reference. The six samples exhibit the same diffraction peaks, which can be indexed to the α-Sr_2SiO_4 phase (JCPDS 39-1256), and no other polymorphs, or other impurities were detected. It is believed that the introduction of Eu^{2+} on the Sr^{2+} sites will induce the phase transition from the β-Sr_2SiO_4 phase to the α-Sr_2SiO_4 phase, so that Eu^{2+} will further stabilize the α-Sr_2SiO_4 phase, which agree with the previous report.[24]

In order to further compare the difference of the phase structure evolution depending on the introduction of the Eu^{2+} and [Lu^{3+}–N^{3-}] chemical unit, the detailed Rietveld structure analysis of the selected Sr_2SiO_4, $Sr_{1.97}Eu_{0.03}SiO_4$ and $Sr_{1.965}Eu_{0.03}$-$Lu_{0.005}SiO_{3.995}N_{0.005}$ samples has been performed. Fig. 2 displays the difference Rietveld plots of Sr_2SiO_4, $Sr_{1.97}Eu_{0.03}SiO_4$ and $Sr_{1.965}Eu_{0.03}Lu_{0.005}SiO_{3.995}N_{0.005}$. It is found that all the peaks of the as-prepared Sr_2SiO_4 compound were indexed by a monoclinic unit cell ($P2_1/n$) with parameters close to β-phase Sr_2SiO_4.

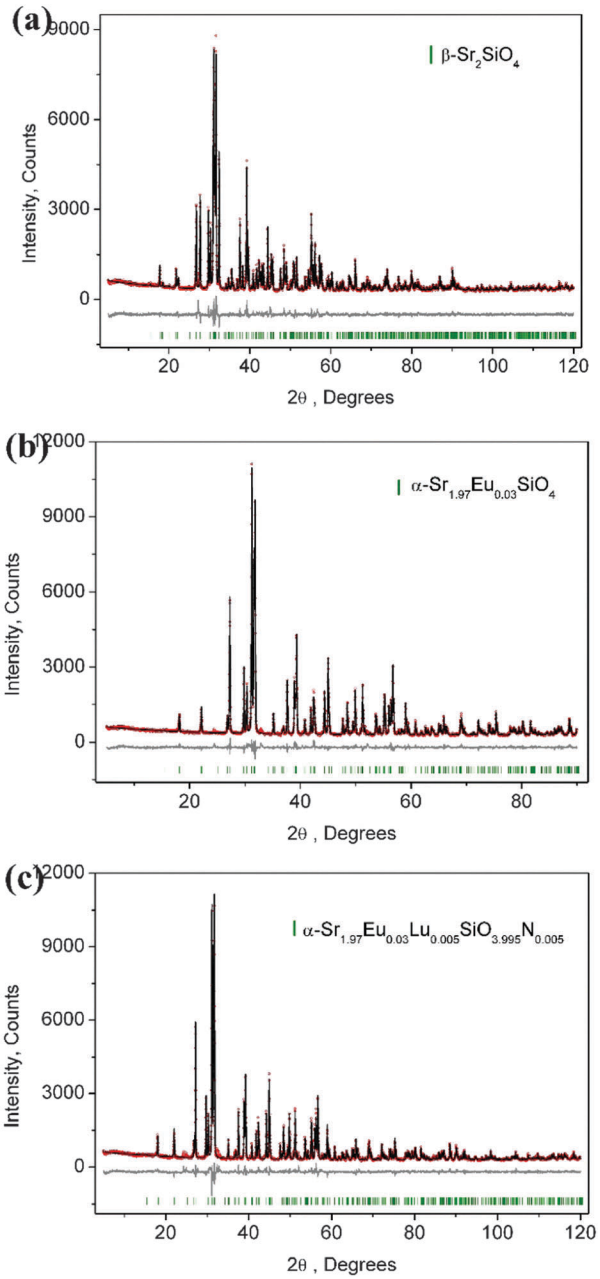

Fig. 2 Powder XRD patterns for Rietveld structural analysis of the selected Sr_2SiO_4 (a), $Sr_{1.97}Eu_{0.03}SiO_4$ (b), and $Sr_{1.965}Eu_{0.03}Lu_{0.005}SiO_{3.995}N_{0.005}$ (c) samples. The solid black lines are calculated intensities, and the red dots are the observed intensities. The short vertical green lines show the position of Bragg reflections of the calculated pattern. The gray solid lines below the profiles stand for the difference between the observed and calculated intensities.

In contrast, all the peaks of $Sr_{1.97}Eu_{0.03}SiO_4$ and $Sr_{1.965}Eu_{0.03}$-$Lu_{0.005}SiO_{3.995}N_{0.005}$ are well fitted by orthorhombic cell (*Pnma*) corresponding to α-phase Sr_2SiO_4. During the Rietveld structural analysis, sites of Sr and O atoms were occupied by Eu/Lu and N atoms with fixed occupations, respectively, according to suggested chemical formula. Refinement was stable and gives low R-factors as shown in Table 1. Moreover, the coordinates of atoms are shown in Table 2, which verified the proposed chemical unit cosubstitution model.

Table 1 Main parameters of processing and refinement of the samples

Compound	Sr_2SiO_4	$Sr_{1.97}Eu_{0.03}SiO_4$	$Sr_{1.965}Eu_{0.03}Lu_{0.005}SiO_{3.995}N_{0.005}$
Sp. gr.	$P2_1/n$	*Pnma*	*Pnma*
a, Å	5.66012(9)	7.07515(9)	7.07370(7)
b, Å	7.0808(1)	5.66437(8)	5.66778(6)
c, Å	9.7547(2)	9.7314(1)	9.7363(1)
β, °	92.594(8)	—	—
V, Å^3	390.55(1)	389.998(9)	390.348(7)
Z	4	4	4
2θ-interval, °	5–120	5–90	5–120
No. of reflections	584	183	326
No. of refined parameters	54	56	59
R_{wp}, %	6.76	6.10	7.14
R_p, %	4.94	4.59	5.32
R_{exp}, %	4.38	4.27	4.44
χ^2	1.54	1.43	1.61
R_B, %	2.34	1.88	2.09

Therefore, the above results verified that the [Lu^{3+}–N^{3-}] chemical unit and the Eu^{2+} ions entered into the crystal lattice of Sr_2SiO_4 can maintain the same phase structures. In the present study, the chemical unit cosubstitution takes place at the cation and coordination anion's sites of the polyhedra simultaneously, not the central tetrahedral sites, which are different from our previous study.[10] The substitution on such a site will have the direct effect on the crystal field environment of doped Eu^{2+}, so that we can possibly find the tunable photoluminescence even if the content of the substituted [Lu^{3+}–N^{3-}] chemical unit is relatively low. In order to clearly demonstrate the proposed chemical unit cosubstitution, the possible atoms'

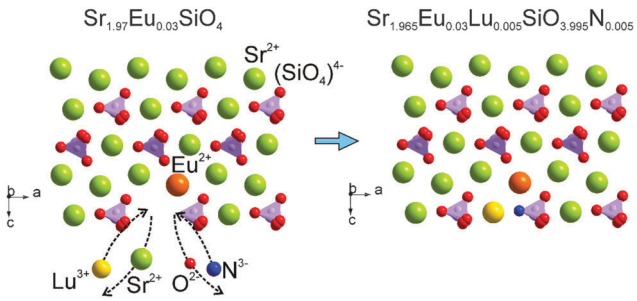

Fig. 3 The proposed chemical unit cosubstitution strategy of [Lu^{3+}–N^{3-}] for [Sr^{2+}–O^{2-}] to highlight the possible atoms' transfer between $Sr_{1.97}Eu_{0.3}SiO_4$ and $Sr_{1.965}Eu_{0.3}Lu_{0.005}SiO_{3.995}N_{0.005}$.

Table 2 Fractional atomic coordinates and isotropic displacement parameters (Å^2) of the samples

	x	y	z	B_{iso}	Occ.
Sr_2SiO_4					
Sr1	0.2624 (3)	0.3429 (2)	0.5783 (2)	1.1 (2)	1
Sr2	0.2699 (3)	0.0009 (2)	0.3021 (2)	1.1 (2)	1
Si	0.2459 (9)	0.7783 (5)	0.5819 (6)	1.0 (2)	1
O1	0.273 (2)	0.005 (1)	0.5739 (8)	1.5 (2)	1
O2	0.196 (2)	0.679 (2)	0.430 (1)	1.5 (2)	1
O3	0.492 (2)	0.682 (2)	0.646 (1)	1.5 (2)	1
O4	0.017 (2)	0.729 (1)	0.673 (1)	1.5 (2)	1
$Sr_{1.97}Eu_{0.03}SiO_4$					
Sr1	0.3409 (2)	0.269 (2)	0.5786 (2)	1.4 (3)	0.4925
Eu1	0.3409 (2)	0.269 (2)	0.5786 (2)	1.4 (3)	0.0075
Sr2	0.9989 (2)	0.271 (1)	0.3036 (1)	0.9 (3)	0.4925
Eu2	0.9989 (2)	0.271 (1)	0.3036 (1)	0.9 (3)	0.0075
Si	0.7780 (6)	0.25	0.5831 (7)	1.5 (3)	1
O1	1.005 (1)	0.300 (3)	0.5657 (9)	1.5 (3)	0.5
O2	0.732 (3)	0.025 (4)	0.674 (2)	1.5 (3)	0.5
O3	0.670 (2)	0.208 (3)	0.433 (1)	1.5 (3)	0.5
O4	0.689 (3)	0.492 (4)	0.647 (2)	1.5 (3)	0.5
$Sr_{1.965}Eu_{0.03}Lu_{0.005}SiO_{3.995}N_{0.005}$					
Sr1	0.3403 (2)	0.268 (1)	0.5794 (2)	1.2 (2)	0.49125
Eu1	0.3403 (2)	0.268 (1)	0.5794 (2)	1.2 (2)	0.0075
Lu1	0.3403 (2)	0.268 (1)	0.5794 (2)	1.2 (2)	0.00125
Sr2	0.9993 (2)	0.230 (1)	0.3023 (2)	0.8 (2)	0.49125
Eu2	0.9993 (2)	0.230 (1)	0.3023 (2)	0.8 (2)	0.0075
Lu2	0.9993 (2)	0.230 (1)	0.3023 (2)	0.8 (2)	0.00125
Si	0.7775 (6)	0.25	0.5828 (7)	1.2 (2)	1
O1	1.005 (1)	0.303 (2)	0.569 (1)	1.5 (2)	0.5
O2	0.736 (3)	0.024 (3)	0.677 (2)	1.5 (2)	0.5
O3	0.670 (2)	0.207 (3)	0.430 (1)	1.5 (2)	0.5
O4	0.685 (3)	0.493 (3)	0.647 (2)	1.5 (2)	0.5

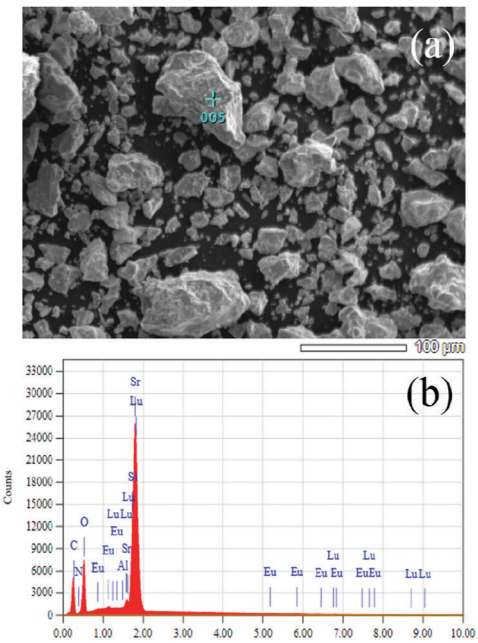

Fig. 4 SEM image (a) and EDS (b) analysis of the selected sample of $Sr_{1.965}Eu_{0.3}Lu_{0.005}SiO_{3.995}N_{0.005}$ to check the presence of existed elements.

transfer between $Sr_{1.97}Eu_{0.3}SiO_4$ and $Sr_{1.965}Eu_{0.3}Lu_{0.005}SiO_{3.995}N_{0.005}$ can be clearly seen in Fig. 3. Two ions Sr^{2+} and O^{2-}, which together have zero sum of charge, are substituted by two ions Lu^{3+} and N^{3-}, which also have zero sum of charge. The scheme can be presented as: $Sr^{2+} + O^{2-} \rightarrow Lu^{3+} + N^{3-}$. From Fig. 3 we can know that the component replacement affects the lattice environment of the luminescence center, and further impacts the spectrum emission of phosphors.[25,26] In order to demonstrate the chemical composition information of the typical samples, SEM-EDS analysis of the typical $Lu_{0.005}Sr_{1.965}SiN_{0.005}O_{3.995}$:0.03$Eu^{2+}$ phosphor for a semi-quantitative measurement has been performed and demonstrated in Fig. 4. As shown in Fig. 4a, the sample has irregular morphology, and when we focused on one minor aggregate for the EDS analysis, we can find that all the elements can be detected, and the contents in the same order of magnitude are in agreement with the designed ones in the chemical formula. Since the doped contents of the Lu/N are very minor, it is difficult to be measured by using the chemical method, so that the present result can also support the successful substitution of the [Lu^{3+}–N^{3-}] couple for [Sr^{2+}–O^{2-}] in the Sr_2SiO_4:Eu^{2+}.

The as-measured and normalized PL spectra of $Lu_xSr_{1.97-x}SiN_xO_{4-x}$:0.03$Eu^{2+}$ (x = 0, 0.0025, 0.00375, 0.005) phosphors under 365 nm excitation are shown in Fig. 5a and b, respectively. The emission spectra consist of an asymmetric broad band

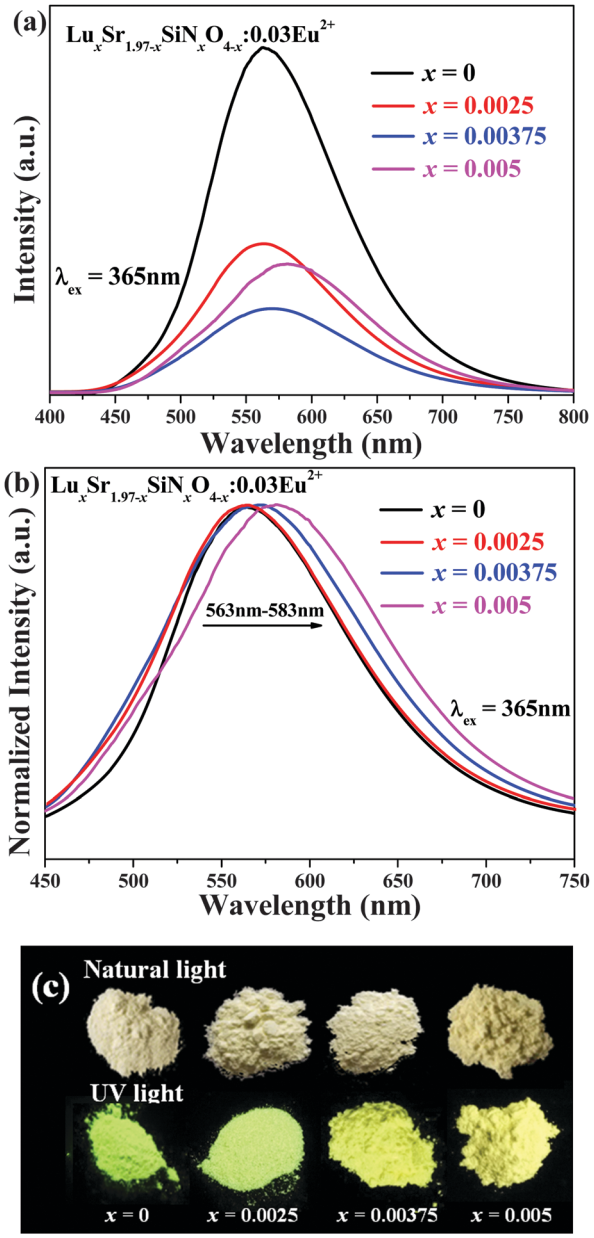

Fig. 5 The as-measured (a) and normalized (b) PL spectra of $Lu_xSr_{1.97-x}SiN_xO_{4-x}$:0.03$Eu^{2+}$ (x = 0, 0.0025, 0.00375 and 0.005) phosphors under 365 nm excitation. (c) Comparative images of $Lu_xSr_{1.97-x}SiN_xO_{4-x}$:0.03$Eu^{2+}$ phosphors under natural light and a 365 nm UV lamp.

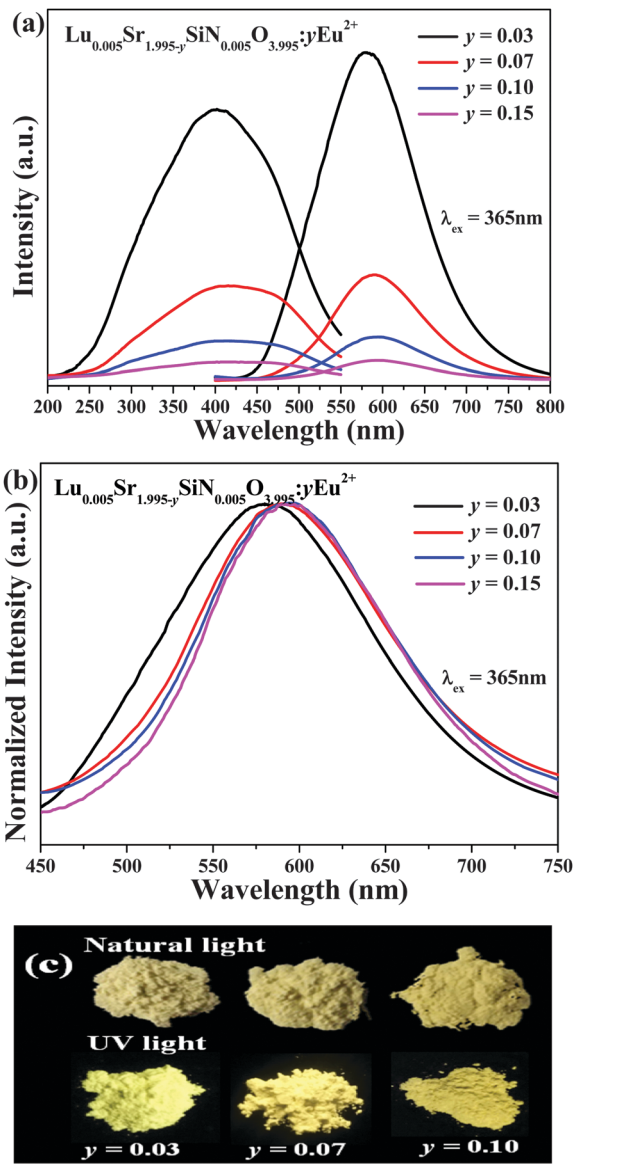

Fig. 6 The as-measured PL and PLE spectra (a) and the normalized PL spectra of $Lu_{0.005}Sr_{1.965-y}SiN_{0.005}O_{3.995}$:y$Eu^{2+}$ (y = 0.03, 0.07, 0.10 and 0.15) phosphors under 365 nm excitation. (c) Comparative images of $Lu_{0.005}Sr_{1.995-y}SiN_{0.005}O_{3.995}$:y$Eu^{2+}$ phosphors under natural light and a 365 nm UV lamp.

centered at around 570 nm, which is ascribed to the electric dipole allowing the transition of the Eu^{2+} ions from the lowest level of the 5d excited state to the 4f ground state.[27] As shown in Fig. 5b (with increasing) [Lu^{3+}–N^{3-}] content, the emission peaks give a red-shift from 563 nm to 583 nm. Fig. 5c comparatively gives the typical images of $Lu_xSr_{1.97-x}SiN_xO_{4-x}$:0.03$Eu^{2+}$ (x = 0, 0.0025, 0.00375 and 0.005) phosphors under a 365 nm UV lamp and natural light, respectively. We can clearly find the emission color evolution from yellow green to yellow with increasing [Lu^{3+}–N^{3-}] content for the cosubstitution of [Sr^{2+}–O^{2-}]. As we know, the N^{3-} is less electronegative and more polarizable than O^{2-} and its introduction in $Sr_{1.97}Eu_{0.03}SiO_4$ increases the covalent character of the bonds with the Sr^{2+}/Eu^{2+}, and we can infer that some of the Eu^{2+} ions in the $Lu_xSr_{1.97-x}SiN_xO_{4-x}$:0.03$Eu^{2+}$ phosphor are coordinated with nitrogen, so that we can find the obvious red-shift behavior.

Fig. 6a shows the as-measured PL and PLE spectra of $Lu_{0.005}Sr_{1.965-y}SiN_{0.005}O_{3.995}$:$yEu^{2+}$ (y = 0.03, 0.07, 0.10 and 0.15) phosphors, and the normalized PL spectra are shown in Fig. 6b. Broad emission bands were clearly observed in the 450–750 nm range for $Lu_{0.005}Sr_{1.965-y}SiN_{0.005}O_{3.995}$:$yEu^{2+}$ phosphors. From Fig. 6b (we can clearly see that) (with increasing) Eu^{2+} concentration, the PL emission peaks show a red-shift from 583 nm to 595 nm. Fig. 6c also presents the images of $Lu_{0.005}Sr_{1.995-y}SiN_{0.005}O_{3.995}$:$yEu^{2+}$ (y = 0.03, 0.07, 0.10 and 0.15) phosphors under a 365 nm UV lamp and natural light, respectively. We can see that the emission color evolves from light yellow to deep yellow with increasing Eu^{2+} doping content. The main reason for this red-shift is an increase of crystal field splitting, which in turn decreases the 5d–4f transition energy.[28]

The temperature dependence of the emission spectra and the relative PL intensity of $Sr_{1.97}SiO_4$:0.03Eu^{2+} and $Lu_{0.005}Sr_{1.965}SiN_{0.005}O_{3.995}$:0.03$Eu^{2+}$ were comparatively investigated and are given in Fig. 7a and b. Furthermore, as shown in Fig. 7c, the emission intensity at 100 °C is about 30% of that measured at room temperature for the $Sr_{1.97}SiO_4$:0.03Eu^{2+} phosphor while this value is about 51% for $Lu_{0.005}Sr_{1.965}SiN_{0.005}O_{3.995}$:0.03$Eu^{2+}$ phosphor. The improved thermal stability depending on the introduced [Lu^{3+}–N^{3-}] chemical unit can be clearly found, which should be ascribed to the enhanced chemical bond effect with a rigid structure originating from the incorporated N atoms and the charge balance originating from such a cosubstitution. In order to better understand the temperature dependence of the luminescence, the activation energy ΔE can be calculated using the following equation:[29]

$$I_T = \frac{I_0}{1 + c\exp\left(-\frac{\Delta E}{kT}\right)} \quad (1)$$

where T is the temperature and c is a constant, k is the Boltzmann constant (8.629 × 10^{-5} eV K^{-1}). I_0 and I_T are the initial PL intensity of the phosphor at room temperature and

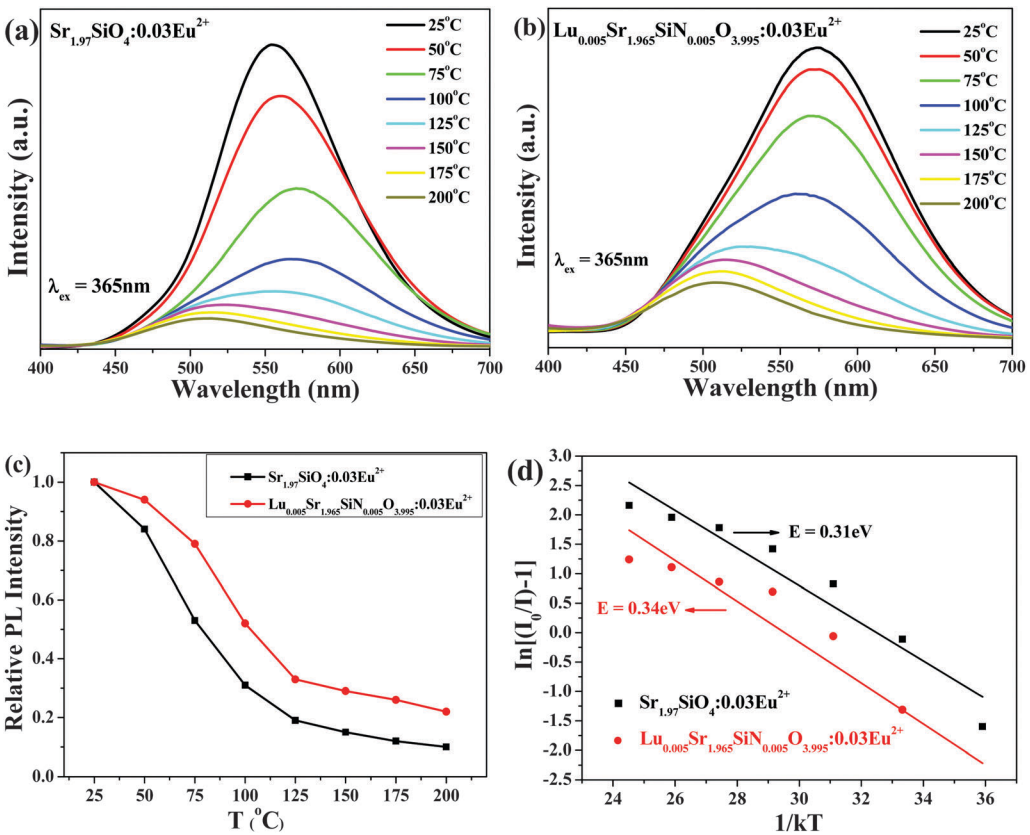

Fig. 7 The temperature dependent emission spectra of $Sr_{1.97}SiO_4$:0.03Eu^{2+} (a) and $Lu_{0.005}Sr_{1.965}SiN_{0.005}O_{3.995}$:0.03$Eu^{2+}$ (b). The temperature dependence of relative PL intensity (c) and the plot of ln[I_0/I − 1] *versus* 1/kT (d) for $Sr_{1.97}SiO_4$:0.03Eu^{2+} and $Lu_{0.005}Sr_{1.965}SiN_{0.005}O_{3.995}$:0.03$Eu^{2+}$ samples.

different temperatures, respectively. A plot of $\ln[I_0/I - 1]$ *versus* $1/kT$ for the $Sr_{1.97}SiO_4$:0.03Eu^{2+} and $Lu_{0.005}Sr_{1.965}SiN_{0.005}O_{3.995}$:0.03$Eu^{2+}$ samples is depicted in Fig. 7d. On the basis of eqn (1), ΔE values of $Sr_{1.97}SiO_4$:0.03Eu^{2+} and $Lu_{0.005}Sr_{1.965}SiN_{0.005}O_{3.995}$:0.03$Eu^{2+}$ samples were estimated to be 0.31 eV and 0.34 eV, respectively. The result further confirms the good thermal stability of $Lu_{0.005}Sr_{1.965}SiN_{0.005}O_{3.995}$:0.03$Eu^{2+}$ phosphors.

Decay curves of Eu^{2+} emission in $Lu_xSr_{1.97-x}SiN_xO_{4-x}$:0.03$Eu^{2+}$ and $Lu_{0.005}Sr_{1.965-y}SiN_{0.005}O_{3.995}$:$yEu^{2+}$ phosphors under excitation at 365 nm, monitored at 563 nm, are shown in Fig. 8. As depicted in Fig. 8a and b, we can find that all the decay curves of Eu^{2+} emission in $Lu_xSr_{1.97-x}SiN_xO_{4-x}$:0.03$Eu^{2+}$ (x = 0, 0.00125, 0.0025, 0.00375 and 0.005) phosphors and $Lu_{0.005}Sr_{1.995-y}SiN_{0.005}O_{3.995}$:$yEu^{2+}$ (x = 0.03, 0.05, 0.07, 0.10 and 0.15) phosphors demonstrate a second-order exponential decay and they can be fitted by this formula:[30]

$$I(t) = I_0 + A_1 \exp(-t/\tau_1) + A_2 \exp(-t/\tau_2) \quad (2)$$

where t is the time, $I(t)$ is the luminescence intensity at time t, A_2 and A_1 are constants, and τ_1 and τ_2 are rapid and slow time for the exponential components. Then we can calculate the average lifetime τ^* by using the formula as follows:

$$\tau^* = (A_1\tau_1^2 + A_2\tau_2^2)/(A_1\tau_1 + A_2\tau_2) \quad (3)$$

The calculated average decay lifetime values of Eu^{2+} ions in $Lu_xSr_{1.97-x}SiN_xO_{4-x}$:0.03$Eu^{2+}$ (x = 0, 0.00125, 0.0025, 0.00375, 0.005) are determined to be 6.98, 6.84, 6.66, 6.48 and 6.24 μs, respectively, depending on the different [Lu^{3+}–N^{3-}] contents. From Fig. 8b we can find that the lifetime values of Eu^{2+} ions are determined to be 6.24, 5.23, 4.27, 3.31 and 1.67 μs for the $Lu_{0.005}Sr_{1.965-y}SiN_{0.005}O_{3.995}$:$yEu^{2+}$ phosphors with y = 0.03, 0.05, 0.07, 0.10 and 0.15, respectively. Obviously the decay time decreases gradually with increasing Eu^{2+} concentration. It is proposed that the nonradiative and self-absorption rate of the internal doped ions evidently increases when activators cross the critical separation between the acceptor (quenching site) and the donor (activator ion) with increasing Eu^{2+} concentration.[31,32]

Fig. 9 shows the CIE chromaticity diagram of the select $Lu_xSr_{1.97-x}SiN_xO_{4-x}$:0.03$Eu^{2+}$ and $Lu_{0.005}Sr_{1.895}SiN_{0.005}O_{3.995}$:0.10$Eu^{2+}$ phosphors (λ_{ex} = 365 nm). The CIE results are listed in Table 3. From Fig. 9, one can see that the emission colors of $Lu_xSr_{2-x-y}SiN_xO_{4-x}$:$yEu^{2+}$ phosphors can be shifted from yellowish green to deep yellow by the chemical unit cosubstitution of [Lu^{3+}–N^{3-}] and the increasing Eu^{2+} doping concentration

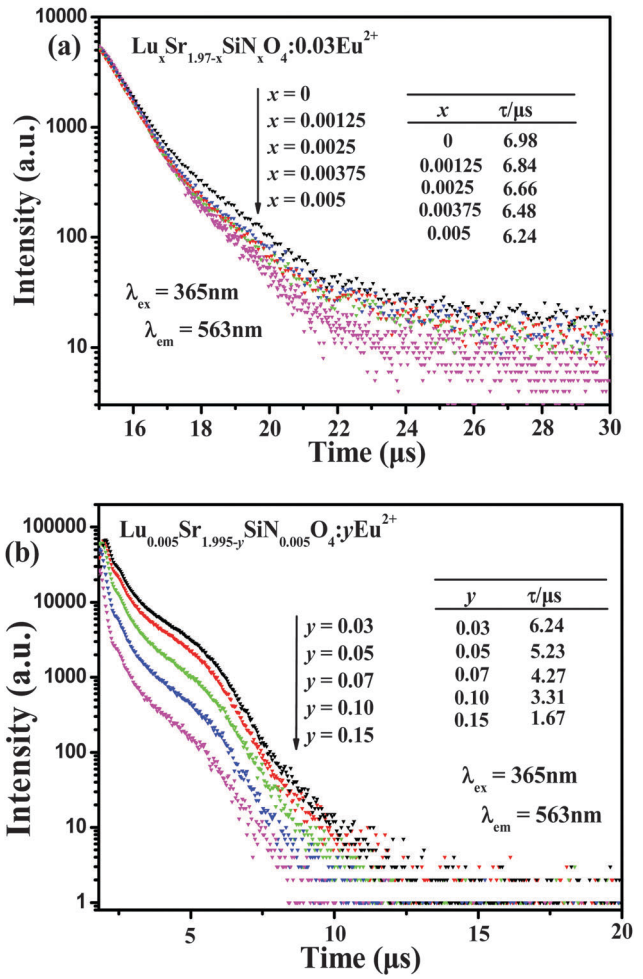

Fig. 8 Decay curves of Eu^{2+} emission in $Lu_xSr_{1.97-x}SiN_xO_{4-x}$:0.03$Eu^{2+}$ (a), $Lu_{0.005}Sr_{1.995-y}SiN_{0.005}O_{3.995}$:$yEu^{2+}$ (b) phosphors monitored at corresponding emission peaks under excitation at 365 nm.

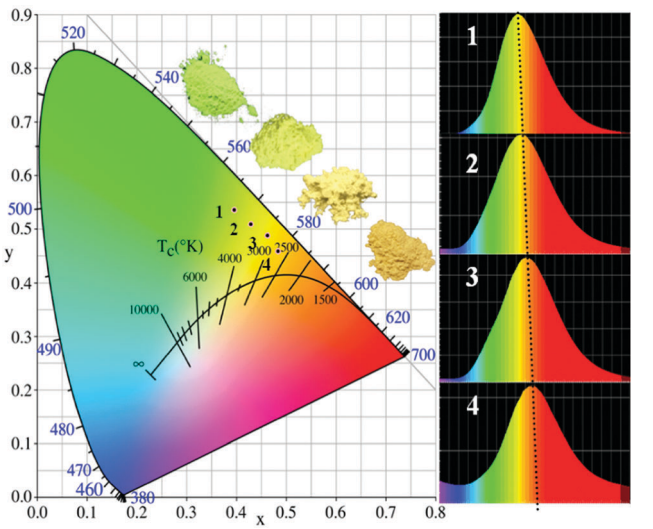

Fig. 9 CIE chromaticity diagram of the select $Lu_xSr_{1.97-x}SiN_xO_{4-x}$:0.03$Eu^{2+}$ (x = 0, 0.0025, 0.005) and $Lu_{0.005}Sr_{1.895}SiN_{0.005}O_{3.995}$:0.10$Eu^{2+}$ phosphors (λ_{ex} = 365 nm).

Table 3 Comparison of the CIE chromaticity coordinates (x, y) for $Lu_xSr_{1.97-x}SiN_xO_{4-x}$:0.03$Eu^{2+}$ (x = 0, 0.0025, 0.005) and $Lu_{0.005}Sr_{1.895}SiN_{0.005}O_{3.995}$:0.10$Eu^{2+}$ phosphors (λ_{ex} = 365 nm)

Sample no.	CIE coordinates (x, y)
1	(0.396, 0.537)
2	(0.428, 0.501)
3	(0.462, 0.488)
4	(0.482, 0.473)

compared to the initial phosphor Sr_2SiO_4:Eu^{2+}. Accordingly, the corresponding CIE coordinates of $Lu_xSr_{2-x-y}SiN_xO_{4-x}$:$yEu^{2+}$ phosphors can be changed from (0.396, 0.537) to (0.482, 0.473). Also on the right side, we can clearly find the red shift trend. The internal quantum efficiency (QE) of the selected $Lu_xSr_{1.97-x}SiN_xO_{4-x}$:$0.03Eu^{2+}$ (x = 0, 0.005) phosphors were measured, and the internal QE values of $Sr_{1.97}SiO_4$:$0.03Eu^{2+}$ and $Lu_{0.005}Sr_{1.965}SiN_{0.005}O_{3.995}$:$0.03Eu^{2+}$ phosphors under 365 nm excitation are determined to be 81.8% and 24.7%, respectively. We can find that the QE values decreased sharply with the introduction of the [Lu^{3+}–N^{3-}] couple, however, it could be improved *via* controlling the particle size, size distribution, morphology and crystalline defects in the future work. Therefore, this series of $Lu_xSr_{2-x-y}SiN_xO_{4-x}$:$yEu^{2+}$ phosphors may be promising candidates as color tunable luminescence materials for application in wLEDs.

4. Conclusions

The effects of [Lu^{3+}–N^{3-}] chemical unit cosubstitution on the phase structures and luminescence properties of $Lu_xSr_{2-x-y}SiN_xO_{4-x}$:$yEu^{2+}$ phosphors were investigated in this paper. The crystal chemistry analysis, also combining with the XRD patterns and PL spectral results, revealed that the [Lu^{3+}–N^{3-}] couple could be incorporated into the Sr_2SiO_4 host *via* cosubstitution with [Sr^{2+}–O^{2-}], which further affects the crystal field environment of doped Eu^{2+} and further tunes the photoluminescence of the as-obtained phosphor. The PL emission reveals a red-shift and the emission color evolution from yellow green to deep yellow with increasing [Lu^{3+}–N^{3-}] substitution content. Accordingly, the CIE coordinates of $Lu_xSr_{2-x-y}SiN_xO_{4-x}$:$yEu^{2+}$ phosphors can be changed from (0.396, 0.537) to (0.482, 0.473). The tunable luminescence properties and high thermal stability demonstrate that $Lu_xSr_{2-x-y}SiN_xO_{4-x}$:$yEu^{2+}$ phosphors can be applied as potential yellow phosphors for wLEDs. The demonstrated chemical unit cosubstitution strategy will also be significant in discovering new systems for advanced optical materials.

Acknowledgements

This work was supported by the National Natural Science Foundation of China (Grant No. 51572023 and 51272242), the Program for New Century Excellent Talents in University of Ministry of Education of China (NCET-12-0950), Beijing Nova Program (Z131103000413047), the Funds of the State Key Laboratory of Rare Earth Resource Utilization, Changchun Institute of Applied Chemistry, CAS (RERU2015022), and Fundamental Research Funds for the Central Universities (FRF-TP-15-003A2).

References

1 R. Potyrailo, K. Rajan, K. Stoewe, I. Takeuchi, B. Chisholm and H. Lam, *ACS Comb. Sci.*, 2011, **13**, 579–633.
2 J. J. Pablo, B. Jones, C. L. Kovacs, V. Ozolins and A. P. Ramirez, *Curr. Opin. Solid State Mater. Sci.*, 2014, **18**, 99–117.
3 C. C. Wu, K. B. Chen, C. S. Lee, T. M. Chen and B. M. Cheng, *Chem. Mater.*, 2007, **19**, 3278–3285.
4 H. P. Ji, Z. H. Huang, Z. G. Xia, M. S. Molokeev, V. V. Atuchin, M. H. Fang and S. F. Huang, *J. Phys. Chem. C*, 2015, **119**, 2038–2045.
5 Z. G. Xia, Y. Y. Zhang, M. S. Molokeev, V. V. Atuchin and Y. Luo, *Sci. Rep.*, 2013, **3**, 3310–3317.
6 S. Schmiechen, P. Strobel, C. Hecht, T. Reith, M. Siegert, P. J. Schmidt, P. Huppertz, D. Wiechert and W. Schnick, *Chem. Mater.*, 2015, **27**, 1780–1785.
7 W. B. Park, N. Shin, K. P. Hong, M. Pyo and K. S. Sohn, *Adv. Funct. Mater.*, 2012, **22**, 2258–2266.
8 W. B. Park, S. P. Singh and K. S. Sohn, *J. Am. Chem. Soc.*, 2014, **136**, 2363–2373.
9 N. Hirosaki, T. Takeda, S. Funahashi and R. J. Xie, *Chem. Mater.*, 2014, **26**, 4280–4288.
10 Z. G. Xia, C. G. Ma, M. S. Molokeev, Q. L. Liu, K. Rickert and K. R. Poeppelmeier, *J. Am. Chem. Soc.*, 2015, **137**, 12494–12497.
11 M. M. Shang, C. X. Li and J. Lin, *Chem. Soc. Rev.*, 2014, **43**, 1372–1386.
12 X. J. Zhang, J. Wang, L. Huang, F. J. Pan, Y. Chen, B. F. Lei, M. Y. Peng and M. M. Wu, *ACS Appl. Mater. Interfaces*, 2015, **7**, 10044–10054.
13 A. Kalaji, M. Mikami and A. K. Cheetham, *Chem. Mater.*, 2014, **26**, 3966–3975.
14 S. H. Miao, Z. G. Xia, M. S. Molokeev, M. Y. Chen, J. Zhang and Q. L. Liu, *J. Mater. Chem. C*, 2015, **3**, 4616–4622.
15 K. S. Sohn, J. H. Hwak, Y. S. Jung, H. X. Yan and M. J. Reece, *J. Electrochem. Soc.*, 2008, **155**, 58–61.
16 Y. X. Gu, Q. H. Zhang, Y. G. Li and H. Z. Wang, *J. Alloys Compd.*, 2011, **509**, 109–112.
17 S. J. Lee, S. H. Hong and Y. J. Kim, *J. Electrochem. Soc.*, 2012, **159**, 163–167.
18 Z. Y. Zhao, Z. G. Yang, Y. R. Shi, C. Wang, B. T. Liu, G. Zhu and Y. H. Wang, *J. Mater. Chem. C*, 2013, **1**, 1407–1412.
19 J. Park, S. J. Lee and Y. J. Kim, *Cryst. Growth Des.*, 2013, **13**, 5204–5210.
20 L. C. Ju, X. Xu, L. Y. Hao, Y. Lin and M. H. Lee, *J. Mater. Chem. C*, 2015, **3**, 1567–1575.
21 X. J. Li, Y. J. Hua, H. P. Ma, D. G. Deng, G. H. Jia and S. Q. Xu, *RSC Adv.*, 2015, **5**, 62659–62669.
22 W. Y. Tian, K. X. Song, F. F. Zhang, P. Zhang, J. X. Deng, J. Jiang, J. M. Xu and H. B. Qin, *J. Alloys Compd.*, 2015, **638**, 249–253.
23 A. P. Black, K. A. Denault, J. Ora-Sole, A. R. Goni and A. Fuertes, *Chem. Commun.*, 2015, **51**, 2166–2169.
24 Z. G. Xia, S. H. Miao, M. Y. Chen, M. S. Molokeev and Q. L. Liu, *Inorg. Chem.*, 2015, **54**, 7684–7691.
25 M. Catti, G. Gazzoni and G. Ivaldi, *Acta Crystallogr., Sect. A: Found. Crystallogr.*, 1992, **38**, 217–220.
26 M. Catti, G. Gazzoni, G. Ivaldi and G. Zanini, *Acta Crystallogr., Sect. B: Struct. Sci.*, 1983, **39**, 674–679.

27 S. H. Miao, Z. G. Xia, J. Zhang and Q. L. Liu, *Inorg. Chem.*, 2014, **53**, 10386–10393.
28 S. S. Wang, W. T. Chen, Y. Li, J. Wang, H. S. Sheu and R. S. Liu, *J. Am. Chem. Soc.*, 2013, **135**, 12504–12507.
29 X. Chen, Z. G. Xia and Q. L. Liu, *Dalton Trans.*, 2014, **43**, 13370–13376.
30 Z. G. Xia, X. M. Wang, Y. X. Wang, L. B. Liao and X. P. Jing, *Inorg. Chem.*, 2011, **50**, 10134–10142.
31 Y. F. Liu, X. Zhang, Z. D. Hao, Y. S. Luo, X. J. Wang and J. H. Zhang, *J. Mater. Chem.*, 2011, **21**, 16379–16384.
32 M. M. Jiao, Y. C. Jia, W. Lv, W. Z. Lv, Q. Zhao, B. Q. Shao and H. P. You, *J. Mater. Chem. C*, 2014, **2**, 90–97.